Sparged but not stirred: Rapid, ADH-NADH oxidase catalyzed deracemization of alcohols in a bubble column

Anderson, Shelby R.; Bommarius, Bettina R.; Woodley, John M.; Bommarius, Andreas S.

Published in:
Chemical Engineering Journal

Link to article, DOI:
10.1016/j.cej.2020.127909

Publication date:
2021

Document Version
Peer reviewed version

Sparged but not stirred: rapid, ADH-NADH oxidase catalyzed deracemization of alcohols in a bubble column

Shelby R. Anderson[#], Bettina R. Bommarius[#], John M. Woodley, Andreas S. Bommarius*

Abstract

We investigate in detail both the deracemization reaction rate and maximum conversion of a *(R,S)*-1-phenylethanol in a bubble column and the deactivation rates of both enzymes involved, alcohol dehydrogenase (ADH) and NADH oxidase (nox2). Instead of the predicted ellipsoidal shape of the bubbles, we observe a spherical shape in all our experiments. Calculated values for the area-specific mass transfer coefficient k_La in sparged, but not stirred, solution ranged from 17 to 87 h^{-1}. We find that minimizing the air-liquid interface over time results in the lowest rate of nox 2 deactivation. The onset of nox2 dissociation beyond the initial 50 h correlates with a tenfold increase in the observed deactivation rate constant. The highest conversion (99%) for deracemizing 50 mM (*R*,*S*)-1-phenylethanol was reached in the shortest reaction time (6 h) if large air bubbles (diameter 2.6 mm) at slow flowrates (5 bubbles/s) were employed. A faster flowrate, which delivers more oxygen per unit time, increased the initial reaction rate but resulted in a slower rate at higher conversions and ultimately incomplete maximum conversion (94%). Reaction rates under sparging were 4-8 times faster than in quiescent solution. Lastly, stirring did not significantly aid conversion (41% vs 37% in quiescent solution after 12h) but caused increased enzyme deactivation (44 h vs 136 h half-life quiescent solution).

Keywords

bubble column, oxygen transfer, enzyme deactivation, NADH oxidase, deracemization

1. INTRODUCTION

1.1 Background

Enzyme-catalyzed oxidation reactions are gaining increasing importance in biotechnology, such as for upgrading of natural carbohydrates and kinetic resolutions of racemic compounds.[1-3] Among available oxidants, only O_2 and H_2O_2 are sufficiently abundant, inexpensive, and safe.[4] Molecular oxygen is the more important oxidant, because exogenous addition of H_2O_2 to enzyme-containing solutions often degrades the enzyme.[5] Importantly, H_2O_2 can advantageously be generated *in situ* via oxidases (S-H + O_2 $\rightarrow$ S-OH + H_2O_2) or monooxygenase reactions (S-H + O_2 + NAD(P)H $\rightarrow$ S-OH + H_2O_2 + $NAD(P)^+$), both requiring molecular oxygen as co-substrate. For example, H_2O_2 can be generated *in situ* via formate oxidase (FOx) or by catalysis of other oxidases, such as alcohol oxidase (AOx) catalysis. Formate oxidase (FOx) catalyzes the conversion of O_2 and formate to H_2O_2 and CO_2.[6-8] Likewise, alcohol oxidase (AOx) catalyzes the oxidation of methanol to formaldehyde (and often further to formate, acting as a dual-action AOx and aldehyde oxidase), and to some extent higher alcohols, notably ethanol, n-propanol, and even n-butanol, to their respective aldehydes.[9] Light-driven biocatalytic oxidation reactions are also of increasing interest.[10]

Another example of biooxidation which is especially relevant in combination with dehydrogenases for kinetic resolutions of racemates is the NADH oxidase-catalyzed reduction of O_2 with the concomitant oxidation of NAD(P)H to $NAD(P)^+$. In particular, the nox2 family of enzymes reduces O_2 to water, with only 0.2-0.8% H_2O_2 leakage, in a four-electron reduction,

generating two $NAD(P)^+$ molecules from NAD(P)H: $O_2 + 2\ NAD(P)H + 2\ H^+ \rightarrow 2\ H_2O + 2\ NAD(P)^+$. The mechanism of nox2 catalysis and deactivation has been previously elucidated by Claiborne.[11] Examples of nox2 enzymes that have been used in catalysis include the enzymes from *Lactobacillus sanfranciscensis*[12, 13], *Lactococcus lactis*[14], and *Lactobacillus plantarum*[15]. Other groups have developed nox2 enzymes from *Lactobacillus brevis*[16], *Lactobacillus pentosus*[17, 18], *Lactobacillus reuteri*[19], *Streptococcus mutans*[20, 21], *Streptococcus pyogenes*[22], and *Giardia lamblia*[23]. The status was summarized recently in a comprehensive review.[24]

NADH oxidase-catalyzed reactions depend on the substrate molecular oxygen (O_2). The oxygen transfer rate (OTR) limits the reaction rate of nox2 and thus the production. Owing to its low solubility in water ($[O_2]_{equ} \approx 0.2$ mM at 25°C and an ionic strength of ≈ 0.2 M)[25], O_2 has to be continually supplied by sparging air (or even pure oxygen) into the solution. Commonly, to maintain small bubbles, the sparged solutions are strongly stirred, to a maximum power input per unit volume P/V of about 3 KW/m^3. Still, the oxygen transfer rate OTR ($OTR = N_{O2} = k_La\ ([O_2]_{equ} - [O_2]_{sol})$, even if $[O_2]_{sol} \rightarrow 0$, cannot exceed 100 mM/h, as the maximally achievable k_La value is around 500 h^{-1} in a vigorously stirred tank ($k_La = 0.026 \cdot (P/V)^{0.4} (v_{rel})^{0.5}$).[26]

While vigorous stirring is usually advantageous in a fermenter with growing (or even resting) cells, it is detrimental when dealing with enzymes in an oxidative biotransformation. Enzyme deactivation as a function of temperature is well understood and has been successfully modeled.[27-29] However, enzymes have also been shown to be sensitive to the secondary effects of shear, interfacial stress at air-liquid and solid-liquid interfaces. In particular, the effects of

stirring have been found to cause unexpectedly large rates of deactivation, as demonstrated in the case of lysozyme[30], formate dehydrogenase[31], and recently for NADH oxidase.[32]

The observed first-order rate constant of deactivation $k_{d,obs}$ for NADH oxidase at 25°C and pH 7 upon stirring is enhanced two-fold over the value in quiescent solution (0.06 vs 0.033 h^{-1})[32]. However, the initial $k_{d,obs}$ value of 0.031 h^{-1} in sparged (although un-stirred) solution in a bubble column is comparable with the value in quiescent solution (0.033 h^{-1}). Thus, sparging does not significantly contribute to enzyme deactivation, while significantly enhancing oxygen transfer. For example, in a bubble column oxygen transfer has been shown to be enhanced six-fold compared to quiescent solution and three-fold over stirred (un-sparged solutions).[32] In the present work, we seek to clarify several important open issues of running enzyme-catalyzed oxidations in bubble columns. 1) We seek to investigate whether the surface area of the bubbles or the volume of air in the bubbles controls the enzyme deactivation rate and conversion of alcohol dehydrogenase (ADH)-NADH oxidase (nox2)-catalyzed oxidations of phenylethanol as a model alcohol substrate. 2) We seek to understand the influence of bubble size, bubble frequency, and k_La on both the initial and final conversion rate of the ADH-nox2-catalyzed oxidation of racemic *(R,S)*-1-phenylethanol. 3) We seek to understand the long-term two-parameter first-order enzyme deactivation observed in the system.

We employ the same model reaction as in previous work[32], the oxidation of racemic *(R,S)*-1-phenylethanol to acetophenone and the same nox2 enzyme, the NoxV analog from *Lactobacillus plantarum* (Figure 1).

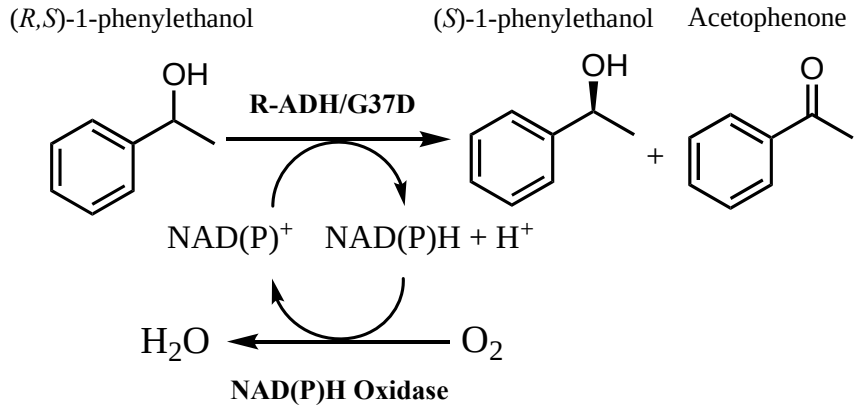

Fig. 1. Alcohol dehydrogenase (ADH)/NADH oxidase (nox2)-catalyzed deracemization of (*R,S*)-phenylethanol.

2. MATERIALS AND METHODS

2.1 Materials used

Potassium phosphate buffer pH 7.0 was used for all solutions. All chemicals used for protein purification were of ACS chemical grade. DTT (Goldbio, St. Louis, MO, USA) was used for nox2 purification. Lysates and partially purified nox2 from *L. plantarum* (NoxV) were prepared as described below. NADH was purchased from VWR (Radnor, PA, USA).

2.2 Enzyme purification

NoxV in pET28a was expressed using BL21 plys cells and overnight express media (VWR, Radnor, PA, USA). Expression was significantly increased by changing the inoculum to a dilution of 1:25, instead of 1:50 as previously used. Cells were harvested at 4000 g (Beckman, Brea, CA, USA) for 20 min and then lysed in 50 mM sodium acetate pH 5.0 + 5 mM DTT. This resulted in much improved lysate which then was further purified using a phenylsepharose FF on an AKTA system and a linear gradient from 2 M to 0 M ammonium sulfate solution, 50 mM Tris buffer at

pH 7.5 and 5 mM DTT. This resulted in a partially purified NoxV enzyme that was more active than that from the previously used purification scheme.[32] (*R*)-ADH (*Lactobacillus brevis*)[33] was purified using IMAC Ni-NTA technology. Control experiments and enzyme activity assays using NAD/ NADH measurements at 340 nm were as described previously.[32]

2.3 Bubble column set-up

The bubble column was a glass tube with a length of 48 cm and an inner diameter of 6.2 mm, as described previously.[32] For the experiments here a few changes were made. Two types of needle (inner diameter 0.39 and 0.22 mm, respectively) were fixed at the bottom of the column operating as a nozzle. Air from the house air supply was sparged through the nozzle at a given flow rate to ensure consistent air flow for longer experiments where the supply from a gas bottle proved insufficient. The air supply line was connected directly to a flow meter and the flow adjusted to reflect either a fast flow (18 bubbles/second) or slow flow (5 bubbles/second).

An I-phone 8 camera in slow motion mode was used to photograph and film the set-up to verify the rising bubble regime and that the bubbles did not touch each other (for video URL, see SI). The bubble diameter (d_b) was established by a photograph of the column that contained a graduated scale: 2.6 mm for large bubbles/large needle and 2.1 mm for small bubbles/small needle. A tube connected to a syringe was installed at the top of the column to fill in the column with the enzyme solution and to collect samples (sample port).

2.4 Procedure

The needle (either 22G or 27G (G = gauge)) was connected to the house air line and inserted into the base of the bubble column. The small 27G needle was additionally punctured through a

gas chromatography septum in the base of the bubble column to prevent leaking. The air valve was opened, and subsequently adjusted to a flow meter setting of approximately '5' for the slow case and '20' for the fast case. The enzyme solution/reaction was slowly added through the sampling port at the top, and the rate (in bubbles/second) was measured using an iPhone camera (Slo-mo 720p at 240 fps). The air flow was adjusted and bubble rate evaluated until the desired rate of 18 bubbles/second for the fast case or 5 bubbles/second for the slow case was achieved.

2.5 Enzyme deactivation

The deactivation constants for nox2 under the four different sparging conditions were evaluated using first-order decay kinetics.[34] Previously, the deactivation profile was consistent with one-parameter first-order decay for experiments run until approximately one half-life. However, longer experiment times showed two-parameter first-order deactivation behavior. Two-phase deactivation schemes have been described by Henley and Sadana[34], in which an enzyme is deactivated to a different, although still active, form and then ultimately deactivates to the final non-active form. While the models described by Henley and Sadana correlate the deactivation parameters in many thermal deactivation experiments, the additional mechanical deactivation or presence of a gas-liquid interface in the sparging conditions likely cause the behavior to deviate from what can be described by a thermal model. Therefore, equations 1 and 2 were used to calculate the two distinct deactivation parameters using the residual activity, a/a_0, and time, t.[35] The experimental enzyme half-life under each condition was determined by interpolation.

$$ln\left(\frac{a}{a_0}\right) = -k_1 t \qquad (1)$$

$$ln\left(\frac{a}{a_0}\right) = -k_2 t \quad (2)$$

2.6 HPLC analysis

For HPLC analysis of product formation and substrate consumption a Phenomenex kinetex 5 µX8-C18 column (5 cm, 2.1 mm) was used with a step gradient starting from 5% methanol to 20% methanol in 10 min, followed by increase to 40% methanol in 2 min. Ketone resolution time was 8 min and alcohol resolution time was 6.5 min. A concentration curve for both ketone and alcohol was incorporated into the method to accurately determine the yield of product during the bubble column reaction. The same substrate and product was used as described and characterized previously.[32]

2.7 Size exclusion chromatography-multi-angle laser light scattering (SEC-MALLS)

Oligomericity status before and after the bubble column experiment was analyzed using the size exclusion chromatography-multi-angle laser light scattering (SEC-MALLS) Omnisec instrument (Malvern, PA) with an SRT SEC-300 column (Sepax, Newark, DE). Samples taken before, and during, the bubble column experiment (following deactivation analysis) were run on the SEC-MALLS and the oligomeric state of the enzyme in question analyzed using four detectors: refractive index, UV at 254 nm, right angle and lower angle light scattering, as well as viscosity. The resulting chromatograms were analyzed using triple detection and dn/dc from sample concentration using BSA as the standard and the Omnisec analysis software version 10.41.

2.8 Dimensionless parameters Re, Eo, Mo

Three dimensionless parameters were calculated to evaluate the bubble shape regime. The bubble Reynolds number was calculated using equation 3, in which d_B is the bubble diameter, u_B is the bubble velocity, ρ_L is the liquid density, and μ_L is the liquid viscosity.[25]

$$Re_B = \frac{d_B u_B \rho_L}{\mu_L} \tag{3}$$

The Eotvos and Morton numbers were calculated from equations in Bubbles, Drops, and Particles by R. Clift, J.R. Grace, and M.E. Weber (equations 4, 5)[36]

$$Eo = \frac{g \Delta \rho d_e^2}{\sigma} \tag{4}$$

$$M = \frac{g \mu^4 \Delta \rho}{\rho_L^2 \sigma^3} \tag{5}$$

where g is gravity, $\Delta\rho$ is the difference between the liquid and gas densities, d_e is the equivalent bubble diameter, and σ is the surface tension.

2.9 Calculation of k_La

The oxygen transfer coefficients, k_La values, were calculated for each sparged bubble column condition using the following equations, as detailed in reference 25.[25] The diameter of a bubble generated at an orifice, d_{Bo}, was calculated using a rearranged balance of the forces of buoyancy and surface tension (equation 6).

$$d_{Bo} = \left(\frac{6\sigma d_o}{g(\rho_L - \rho_G)}\right)^{1/3} \quad (6)$$

where d_o is the diameter of the orifice, specifically the inner diameter of the needle.

The experimental flow rate was operated below the transitional gas flow rate, Q_T. Below Q_T, the region is considered constant volume, variable frequency, and the bubble size generated at the orifice is assumed the bubble size in the entirety of the column ($d_{Bo} = d_B$). Verification of operation below the Q_T required calculating the velocity of the bubble at the orifice, u_B, using the Mendleson relationship in equation 7 (for Re >>1).

$$u_{Bo} = \left(\frac{2\sigma}{\rho_L d_{Bo}} + \frac{g d_{Bo}}{2}\right)^{0.5} \quad (7)$$

Therefore, all parameters were calculated to confirm if the experimental gas flow was beneath the transitional gas flow value, Q_T using equation 8. For the large and small bubble conditions, the transitional gas flow values were 0.40 cm^3/s and 0.24 cm^3/s, respectively.

$$Q_T = 0.38 g^{1/2} \left(\frac{6\sigma d_o}{g(\rho_L - \rho_G)}\right)^{5/6} \quad (8)$$

The experiments for bubble column with a constant volume, variable frequency, are indicative of operation below the Q_T. Each bubble has the same size and velocity per needle size, however, changing the gas flow rate changes the frequency at which bubbles enter the column over the time course. The superficial gas velocity, u_s, is calculated by equation 9, using the experimental volumetric gas flow rate, Q, and the bubble column diameter, D_T.

$$u_s = \frac{4Q}{\pi D_T^2} \quad (9)$$

Subsequently, the k_L value is calculated using the literature diffusivity of oxygen in air-water systems, $D_{O2} = 2 \times 10^{-5}$ cm^2/s, and the previously calculated u_{Bo} and d_B in equation 10.

$$k_L = \left[\frac{4D_{O2}u_{Bo}}{\pi d_B}\right]^{1/2} \quad (10)$$

Holdup, ϕ, and interfacial area per unit liquid volume, a, are the final parameters calculated to determine the theoretical k_La constants for each sparged bubble column condition.

$$\phi = \frac{u_s}{u_{Bo}} = \frac{4Q/(\pi D_T^2)}{u_{Bo}} \quad (11)$$

$$a = \frac{6\phi}{d_B} \quad (12)$$

3. RESULTS AND DISCUSSION

3.1 Sparging conditions

The low aqueous solubility of the co-substrate oxygen in the ADH/nox2-catalyzed deracemization of (*R*,*S*)-1-phenylethanol necessitates sparging of air (or pure oxygen) into solution, which itself requires understanding the effects of interfacial area exposure over time on

enzyme deactivation. We tested four sparging conditions in a bubble column, varying both bubble size and gas flowrate. Small bubbles of 2.1 mm diameter were generated with a 27-gauge needle of 0.22 mm inner diameter, and large bubbles of 2.6 mm diameter with a 22-gauge needle of 0.39 mm inner diameter. For the 'fast' and 'slow' gas flowrate, the bubble rates were fixed at 18 and 5 bubbles per second, respectively. Table 1 details the interfacial area and volumetric flowrates, k_La values, and resulting dimensionless numbers for the four experimental sparging conditions. Not surprisingly, calculated k_La values correlate tightly with interfacial area per unit time (A/t), less with gas volume per unit time (V/t).

Table 1

Air bubble properties in the bubble column experiments, for the quiescent liquid phase, pH 7, 25^{o}C; gaseous phase: air, 1.013 bar. Bubble diameter: small/large: 2.1/2.6 mm. Flow rate: fast/slow: 18/5 bubbles/second. The experimental parameters ensured bubbles with constant volume variable frequency, both conditions operating well below Q_T. The k_La values for a constant volume, variable frequency bubble column conditions with flow rate equal to the Q_T range from 217 h^{-1} for large bubbles to 172 h^{-1} for small bubbles.

Condition	**Interfacial Area Rate (cm^2/min)**	**Volumetric Flow Rate (Q) (cm^3/min)**	**Re**	**Eo**	**M**	**k_La (h^{-1})**
Sparged, Large Bubbles, Slow Flow Rate	61.08	2.64	958	0.92	6.6E-12	23.9
Sparged, Large Bubbles, Fast Flow Rate	223.96	9.70	958	0.92	6.6E-12	87.5
Sparged, Small Bubbles, Slow Flow Rate	40.95	1.45	840	0.61	6.6E-12	17.1
Sparged, Small Bubbles, Fast Flow Rate	150.16	5.32	840	0.61	6.6E-12	62.6

Videos demonstrated sphericity and non-coalescence of the bubbles throughout the experiments (SI, dropbox link). The calculated Reynolds (Re), Morton (Mo), and Eötvös (Eö) numbers suggest an ellipsoidal shape of the bubbles when placed into a diagram of bubble shapes (SI, Figure S4).[37] However, the boundaries between shape regimes are rather arbitrary[36] and our results indicate that the diagram needs to be modified when working with gas bubbles in aqueous solution.

3.2 Nox deactivation

Previously, we have reported that nox2 deactivation follows first-order kinetics.[32] However, owing to running out of air (from tanks) during deactivation of more stable samples, we could only observe deactivation for about one half-life. In the present work, given a stable air supply, we consistently observed deviations from simply one parameter first-order deactivation behavior beyond the initial time periods. Instead, the results show a two-parameter first-order deactivation pattern. However, multistep deactivation models ($E_1 \leftrightarrow E_2 \rightarrow D$), in which the native enzyme E_1 unfolds to a different, although still active form E_2, after which it proceeds to the inactive form D,[34] were not an accurate fit for the long-time data taken from the present experiments, likely because the models are based on thermally based deactivation and do not take into account mechanical deactivation forces such as sparging. Therefore, the observed deactivation constants presented in Table 2 were determined from two distinct, independent linear first-order decay model fits, in which the slopes of each line are $k_{d1,observed}$ and $k_{d2,observed}$, respectively. Figure 2 demonstrates first-order deactivation over the time course of each experiment.

Nox2 half-lives, determined at half the initial activity, regardless of whether that time point falls into the first or second branch of the decay curve, were shortest in the presence of small bubbles at fast flowrate ($t_{1/2}$ = 39 h), followed by large bubbles at fast flowrate ($t_{1/2}$ = 56 h) and small bubbles at slow air flow rate ($t_{1/2}$ = 74 h), while the longest half-life was found for large bubbles at slow flow rate ($t_{1/2}$ = 76 h). For the control experiments, stirring caused faster nox2 deactivation ($t_{1/2}$ = 44 h) than quiescent conditions ($t_{1/2}$ = 136 h). Thus, importantly, smaller bubbles and faster flow caused higher rates of Nox2 deactivation than larger bubbles and slower flow, although the effect of flow rate dominates.

Table 2

Nox2 half-lives, transition times between the first and second phase of the deactivation, and deactivation constants at the four different sparging conditions. The transition times occur before the time point of one half life, i.e. after loss of 33 to 45% of initial activity, but follow the same trend. See SI, Table S2 for the estimated standard deviation of the residuals for each linear regression prediction and of the deactivation coefficient in the two-parameter first-order deactivation profiles.

Condition	**Exp. Nox2 Half Life $t_{1/2}$ (h)**	**Transition Time (h)**	**$k_{d1,obs}$ (h^{-1})**	**$k_{d2,obs}$ (h^{-1})**
Sparged, Large Bubbles, Slow Flow Rate	76	58	-0.006	-0.020
Sparged, Small Bubbles, Slow Flow Rate	73	53	-0.003	-0.032
Sparged, Large Bubbles, Fast Flow Rate	56	52	-0.007	-0.071
Sparged, Small Bubbles, Fast Flow Rate	39	29	-0.013	-0.033

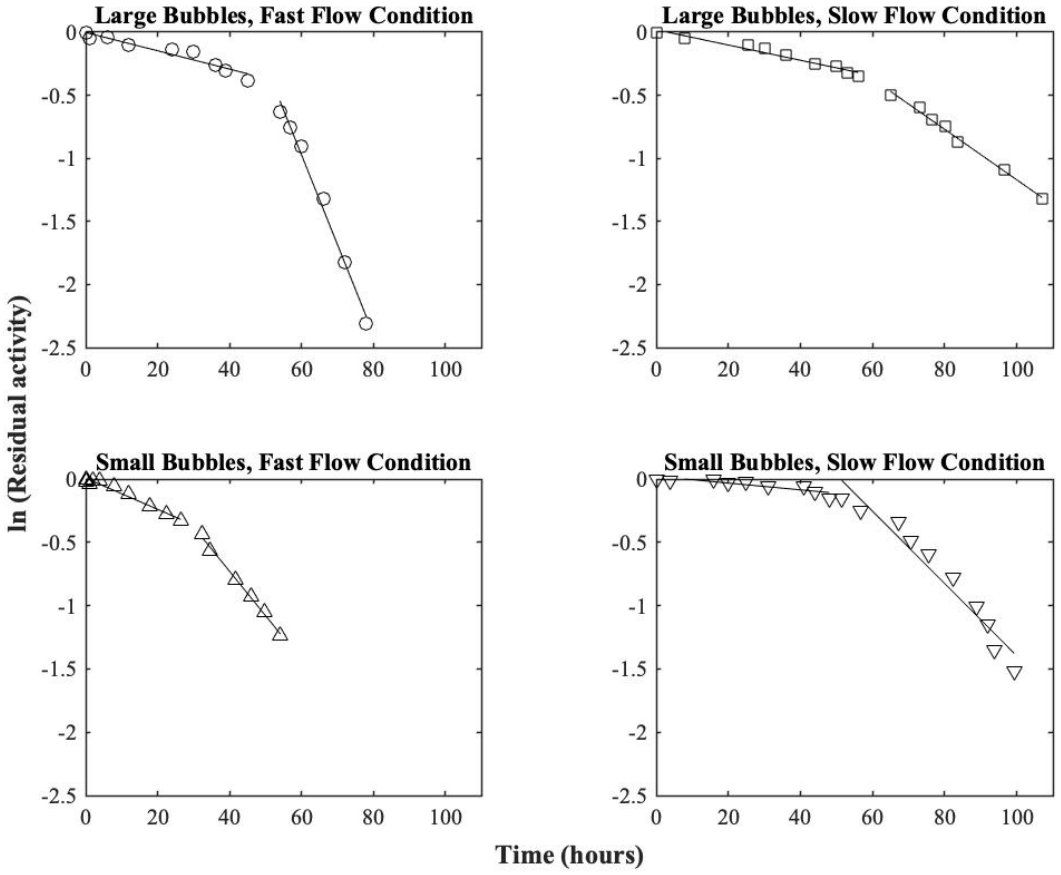

Fig. 2. Deactivation of Nox2 over time in a semilogarithmic plot. Deviations from one parameter first-order deactivation at long times are clearly discernible. Two-parameter first-order deactivation is observed, as shown by two distinct slopes for each condition.

The rate of air supplied to the system seems to affect Nox2 deactivation more than bubble size d_B, gas-liquid interfacial area per unit time (A/t), or gas volumetric flow rate (Q_t = V/t). Slow gas flow rates lead to slower deactivation and thus longer half-lives. While the observed first-branch deactivation rate constant $k_{d1,observed}$ roughly correlates with interfacial area per unit time (A/t), the second branch quantity $k_{d2,observed}$ does not. Therefore, a strategy to minimize Nox2 deactivation is to decrease the rate of gas bubbles rising in the liquid.

To investigate the possible cause for the enhanced deactivation at long times, samples of a running bubble column with Nox2 were analyzed for the presence of oligomeric structures using size exclusion chromatography coupled with multi-angle laser light scattering (SEC-MALLS). A sample taken at one half-life still showed the expected dimer present for Nox2, but a sample taken after loss of activity only showed the MW expected for that of the monomer (SI, Figure S2). In both cases, the small observed amount of aggregated protein ruled out aggregation as the main cause of activity loss. Rather, the loss of quaternary structure, i.e. dissociation of the dimer, due to either the presence of a hydrophobic gas-liquid interface or due to shear of the moving bubbles seems to lead to accelerated deactivation at long times. The apparent onset of dissociation at around one half-life might explain the improved fit of Nox2 activity-time data with two slopes in a semilogarithmic plot (Figure 2).

3.3 ADH/NOX-catalyzed conversion

The four sparging conditions, as well as stirred and quiescent conditions, were analyzed for their ability to drive product formation in the (*R*)-ADH/nox2-catalyzed deracemization of (*R*,*S*)-1-phenylethanol (Figure 1).

The sparging conditions were evaluated for their ability to facilitate oxygen transfer for co-factor regeneration, and thus drive reaction conversion, while minimizing enzyme deactivation due to the air-water interface and overoxidation of the Cys 42 residue during turnover. We analyzed the conversion-time plots with respect to both maximum conversion (important for the enantiomeric purity of the residual enantiomer) and initial rate. We noted that the configuration with the highest initial rate does not finish with the highest degree of conversion (Figure 3). The

configurations with fast flow rate, both with large and small bubbles, have highest initial reaction rate, but do not have the highest overall conversion. Fast flow, both with large and small bubbles, transports the most air through the bubble column in terms of both interfacial area rate and volumetric flow rate (Table 1) and consequently results in the highest initial reaction rates correlating to the highest k_La values. These cases were able to reach 94% maximum conversion in 8 hours and 90% maximum conversion in 7 hours, respectively. In contrast, large bubbles at a slow air flowrate leads to both the third highest k_La value and the third fastest initial reaction rate but resulted in the highest overall conversion at 99%, in the shortest period of time (6 hours). Even the small bubbles at slow air flow rate reached 97% conversion, albeit in 12 hours. Quiescent solutions were able to reach a reaction conversion of 93% in 48 h, which is 4-8 times slower than with the sparging conditions. Stirring provided only a marginally faster reaction rate (both initial and at high conversion), than the quiescent condition. Both stirred and quiescent conditions strongly lagged sparged conditions with respect to conversion at all time points.

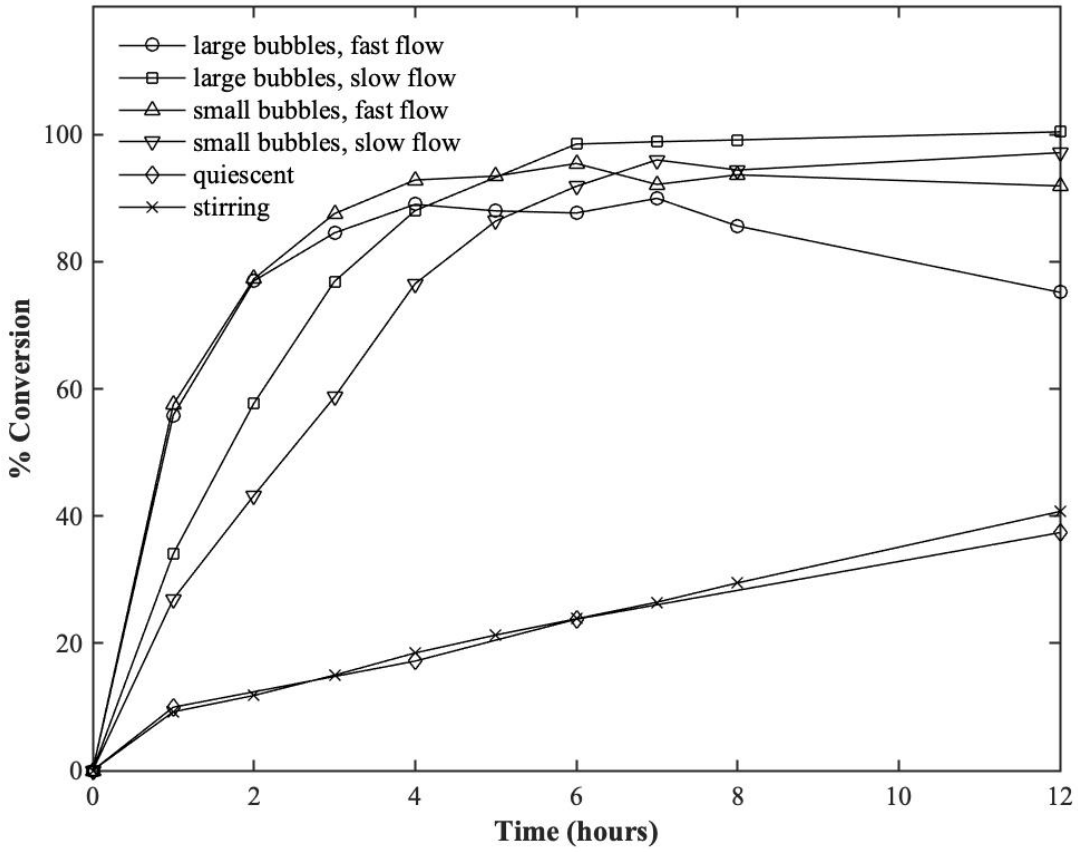

Fig. 3. Acetophenone formation under different bubble column condition in relation to stirred or quiescent solution, monitored via HPLC analysis.

Table 3. Overview of ADH/Nox2-catalyzed conversion of 1-phenylethanol to acetophenone and (*S*)-1-phenylethanol. Reaction conditions: [(*R*,*S*)-1-phenylethanol]: 50 mM, [NAD^+]: 1 mM, pH 7.0, 25^{o}C. *Note: No additional data taken after 36 hours for the stirred condition.

Condition	Max. conversion (%)	Time to max. conversion (h)
Sparged, Large Bubbles, Slow Flow Rate	99	6
Sparged, Small Bubbles, Slow Flow Rate	97	12
Sparged, Small Bubbles, Fast Flow Rate	94	8
Sparged, Large Bubbles, Fast Flow Rate	90	7

Quiescent	93	48
Stirred	82	36*

At the point of maximum conversion, i.e. after 6-12 h for the sparged conditions, Nox2 deactivation is not yet very significant (Table 2). The half-life of deactivation of the *Lactobacillus brevis* (*R*)-ADH for the best case conversion (sparged, large bubbles, slow flow rate) was found to be 76 h, nearly identical to the value for Nox2, while the value at stirred but not sparged conditions was significantly lower than that for Nox2 (19.8 vs 44 h, Suppl. Fig S1). Thus, *L. b.*-(*R*)-ADH deactivation at the points of maximum conversion for sparged conditions also is not very significant.

4. CONCLUSION

Our results demonstrate that operating a bubble column in the constant volume, variable frequency bubble regime enables k_La values up to 87 h^{-1}. In slight contrast to predictions, we only observed spherical, non-coalescing bubbles in that regime. Nox2 deactivation depends on bubble size and sparging frequency: slow flow rates, much more so than large bubble size, dramatically lowered Nox2 deactivation rates. This finding suggests that minimization of gas hold-up, and thus also of the air-liquid interface over time, is a successful strategy to fight enzyme deactivation. Nox2 dissociation at reaction long times seems to vastly increase deactivation as well, resulting in two-parameter first-order deactivation plots.

Running ADH/Nox2-catalyzed deracemization of racemic alcohols in the bubble column, high k_La strongly correlated with high initial reaction rate, up to 2-3 h and 60-85% conversion, thus

demonstrating oxygen transfer as the rate-limiting step. However, sparging large bubbles at a slow flowrate (third-highest k_La) yielded the highest degree of conversion (99%) in the shortest time of all runs (6 h). Thus, high k_La did not correlate with a high final degree of conversion; conversion ≥ 98-99% in deracemizations is required to result in sufficiently high enantiomeric excess of the residual enantiomer. As the half-lives of deactivation $t_{1/2}$ for both Nox2 and ADH at all sparged conditions (35-76 h) significantly exceeded the times to maximum conversion (6-12 h), enzyme deactivation cannot explain low rates at high conversion.

Stirring *in lieu* of sparging or even running reactions in quiescent solution, however, results in excessively long reaction times (≥ 48 h) and ≤ 93% conversion but also in enhanced deactivation in the case of stirring ($t_{1/2}$ = 44 h). Consequently, our results confirm that sparging air into the quiescent liquid of a bubble column in the case of ADH/Nox2-catalyzed deracemization of racemic alcohols enables much higher rates and significantly higher extents of final conversion, at minimal deactivation, in comparison to quiescent or stirred but unsparged controls.

5. ACKNOWLEDGEMENTS

B.R.B., S.R.A., and A.S.B. gratefully acknowledge financial support from the National Science Foundation of the United States (NSF) grant IIP-1540017, A.S.B. also gratefully acknowledges financial support from NSF grant CBET-1512848.

REFERENCES

[1] J. Dong, E. Fernandez-Fueyo, F. Hollmann, C.E. Paul, M. Pesic, S. Schmidt, Y. Wang, S. Younes, W. Zhang, Biocatalytic Oxidation Reactions: A Chemist's Perspective, Angew Chem Int Ed Engl 57 (2018) 9238-9261.

[2] S. Schulz, M. Girhard, V.B. Urlacher, Biocatalysis: Key to Selective Oxidations, ChemCatChem 4 (2012) 1889-1895.

[3] F. Hollmann, I.W.C.E. Arends, K. Buehler, A. Schallmey, B. Bühler, Enzyme-mediated oxidations for the chemist, Green Chemistry 13 (2011) 226-265.

[4] R. Noyori, M. Aoki, K. Sato, Green oxidation with aqueous hydrogen peroxide, Chemical Communications (2003) 1977-1986.

[5] K. Seelbach, M.P.J. van Deurzen, F. van Rantwijk, R.A. Sheldon, U. Kragl, Improvement of the total turnover number and space-time yield for chloroperoxidase catalyzed oxidation, Biotechnology and Bioengineering 55 (1997) 283-288.

[6] F. Tieves, S.J. Willot, M. van Schie, M.C.R. Rauch, S.H.H. Younes, W. Zhang, J. Dong, P. Gomez de Santos, J.M. Robbins, B. Bommarius, M. Alcalde, A.S. Bommarius, F. Hollmann, Formate Oxidase (FOx) from Aspergillus oryzae: One Catalyst Enables Diverse H2 O2 - Dependent Biocatalytic Oxidation Reactions, Angew Chem Int Ed Engl 58 (2019) 7873-7877.

[7] J.M. Robbins, A.S. Bommarius, G. Gadda, Mechanistic studies of formate oxidase from Aspergillus oryzae: A novel member of the glucose-Methanol-choline oxidoreductase enzyme superfamily that oxidizes carbon acids, Arch Biochem Biophys 643 (2018) 24-31.

[8] J.M. Robbins, J. Geng, B.A. Barry, G. Gadda, A.S. Bommarius, Photoirradiation Generates an Ultrastable 8-Formyl FAD Semiquinone Radical with Unusual Properties in Formate Oxidase, Biochemistry 57 (2018) 5818-5826.

[9] M. Pickl, M. Fuchs, S.M. Glueck, K. Faber, The substrate tolerance of alcohol oxidases, Appl Microbiol Biotechnol 99 (2015) 6617-6642.

[10] S. Kochius, Y. Ni, S. Kara, S. Gargiulo, J. Schrader, D. Holtmann, F. Hollmann, Light-Accelerated Biocatalytic Oxidation Reactions, 79 (2014) 1554-1557.

[11] T.C. Mallett, D. Parsonage, A. Claiborne, Equilibrium Analyses of the Active-Site Asymmetry in Enterococcal NADH Oxidase: Role of the Cysteine-sulfenic Acid Redox Center, Biochemistry 38 (1999) 3000-3011.

[12] B.R. Riebel, P.R. Gibbs, W.B. Wellborn, A.S. Bommarius, Cofactor Regeneration of both NAD+ from NADH and NADP+ from NADPH:NADH Oxidase from Lactobacillus sanfranciscensis, Advanced Synthesis & Catalysis 345 (2003) 707-712.

[13] G.T. Lountos, R. Jiang, W.B. Wellborn, T.L. Thaler, A.S. Bommarius, A.M. Orville, The Crystal Structure of NAD(P)H Oxidase from Lactobacillus sanfranciscensis: Insights into the Conversion of O2 into Two Water Molecules by the Flavoenzyme, Biochemistry 45 (2006) 9648-9659.

[14] R. Jiang, B.R. Riebel, A.S. Bommarius, Comparison of Alkyl Hydroperoxide Reductase (AhpR) and Water-Forming NADH Oxidase from Lactococcus lactis ATCC 19435, Advanced Synthesis & Catalysis 347 (2005) 1139-1146.

[15] J.T. Park, J.-I. Hirano, V. Thangavel, B.R. Riebel, A.S. Bommarius, NAD(P)H oxidase V from Lactobacillus plantarum (NoxV) displays enhanced operational stability even in absence of reducing agents, Journal of Molecular Catalysis B: Enzymatic 71 (2011) 159-165.

[16] B. Geueke, B. Riebel, W. Hummel, NADH oxidase from Lactobacillus brevis: a new catalyst for the regeneration of NAD, Enzyme and Microbial Technology 32 (2003) 205-211.

[17] C. Nowak, B. Beer, A. Pick, T. Roth, P. Lommes, V. Sieber, A water-forming NADH oxidase from Lactobacillus pentosus suitable for the regeneration of synthetic biomimetic cofactors, Front Microbiol 6 (2015) 957.

[18] J.-D. Zhang, Z.-M. Cui, X.-J. Fan, H.-L. Wu, H.-H. Chang, Cloning and characterization of two distinct water-forming NADH oxidases from Lactobacillus pentosus for the regeneration of NAD, Bioprocess and Biosystems Engineering 39 (2016) 603-611.

[19] T. Dishisha, R. Sabet-Azad, V. Arieta, R. Hatti-Kaul, Lactobacillus reuteri NAD(P)H oxidase: Properties and coexpression with propanediol-utilization enzymes for enhancing 3-hydroxypropionic acid production from 3-hydroxypropionaldehyde, J Biotechnol 289 (2019) 135-143.

[20] B. Petschacher, N. Staunig, M. Muller, M. Schurmann, D. Mink, S. De Wildeman, K. Gruber, A. Glieder, Cofactor Specificity Engineering of Streptococcus mutans NADH Oxidase 2 for NAD(P)(+) Regeneration in Biocatalytic Oxidations, Comput Struct Biotechnol J 9 (2014) e201402005.

[21] F.-L. Li, F.-L. Li, Y. Shi, J.-X. Zhang, J. Gao, Y.-W. Zhang, Cloning, expression, characterization and homology modeling of a novel water-forming NADH oxidase from Streptococcus mutans ATCC 25175, Int J Biol Macromol 113 (2018) 1073-1079.

[22] H. Gao, M.K. Tiwari, R.K. Singh, B.H. Sung, S.C. Kim, J.K. Lee, Role of surface residue 184 in the catalytic activity of NADH oxidase from Streptococcus pyogenes, Appl Microbiol Biotechnol 98 (2014) 7081-7088.

[23] A. Castillo-Villanueva, S.T. Mendez, A. Torres-Arroyo, H. Reyes-Vivas, J. Oria-Hernandez, Cloning, Expression and Characterization of Recombinant, NADH Oxidase from Giardia lamblia, Protein J 35 (2016) 24-33.

[24] G. Rehn, A.T. Pedersen, J.M. Woodley, Application of NAD(P)H oxidase for cofactor regeneration in dehydrogenase catalyzed oxidations, Journal of Molecular Catalysis B: Enzymatic 134 (2016) 331-339.

[25] H.W. Blanch, D.S. Clark, Biochemical engineering, M. Dekker, New York, 1996.

[26] K. Van't Riet, Review of Measuring Methods and Results in Nonviscous Gas-Liquid Mass Transfer in Stirred Vessels, Industrial & Engineering Chemistry Process Design and Development 18 (1979) 357-364.

[27] T.A. Rogers, A.S. Bommarius, Utilizing simple biochemical measurements to predict lifetime output of biocatalysts in continuous isothermal processes, Chemical Engineering Science 65 (2010) 2118-2124.

[28] R.M. Daniel, M.J. Danson, A new understanding of how temperature affects the catalytic activity of enzymes, 35 (2010) 584-591.

[29] R.M. Daniel, M.J. Danson, R. Eisenthal, The temperature optima of enzymes: a new perspective on an old phenomenon, Trends in Biochemical Sciences 26 (2001) 223-225.

[30] S. Colombié, A. Gaunand, M. Rinaudo, B. Lindet, Irreversible lysozyme inactivation and aggregation induced by stirring: kinetic study and aggregates characterisation, Biotechnology Letters 22 (2000) 277-283.

[31] A.S. Bommarius, A. Karau, Deactivation of formate dehydrogenase (FDH) in solution and at gas-liquid interfaces, Biotechnol Prog 21 (2005) 1663-1672.

[32] M. Dias Gomes, B.R. Bommarius, S.R. Anderson, B.D. Feske, J.M. Woodley, A.S. Bommarius, Bubble Column Enables Higher Reaction Rate for Deracemization of (R,S)-1-Phenylethanol with Coupled Alcohol Dehydrogenase/NADH Oxidase System, Advanced Synthesis & Catalysis 361 (2019) 2574-2581.

[33] N.H. Schlieben, K. Niefind, J. Muller, B. Riebel, W. Hummel, D. Schomburg, Atomic resolution structures of R-specific alcohol dehydrogenase from Lactobacillus brevis provide the structural bases of its substrate and cosubstrate specificity, J Mol Biol 349 (2005) 801-813.

[34] J.P. Henley, A. Sadana, Deactivation theory, Biotechnology and Bioengineering 28 (1986) 1277-1285.

[35] X. Feng, H. Tang, B. Han, B. Lv, C. Li, Enhancing the Thermostability of β-Glucuronidase by Rationally Redesigning the Catalytic Domain Based on Sequence Alignment Strategy, Industrial & Engineering Chemistry Research 55 (2016) 5474-5483.

[36] R. Clift, J.R. Grace, M.E. Weber, Bubbles, drops, and particles, Academic Press, New York, 1978.

[37] E.D. Johnson, S. Middleman, Elongational flow of polymer melts, Polymer Engineering & Science 18 (1978) 963-968.